Equilibrium properties of a grafted polyelectrolyte with explicit counterions

Kandiledath Jayasree,[1,a)] P. Ranjith,[2,b)] Madan Rao,[3,c)] and P. B. Sunil Kumar[1,d)]

[1]*Department of Physics, Indian Institute of Technology Madras, Chennai-600036, India*
[2]*Physico-Chimie UMR 168, Institut Curie, 26 rue d'Ulm, 75248 Paris Cedex 05, France*
[3]*Raman Research Institute, Bangalore-560080, India and National Center for Biological Sciences (TIFR), GKVK Campus, Bangalore-560065, India*

We study the equilibrium conformations of a grafted polyelectrolyte (PE) in the presence of explicit counterions (CIs) using Monte Carlo simulations. The interplay between attractive Lennard-Jones interactions (parametrized by ϵ) and electrostatics (parametrized by $A = q^2 l_B / a$, where q is the CI valency, l_B is the Bjerrum length, and a is the monomer diameter) results in a variety of conformations, characterized as extended (E), pearls with m beads (P_m), sausage (S), and globular (G). For large ϵ, we observe a transition from $G \rightarrow P_2 \rightarrow P_3 \rightarrow \ldots \rightarrow S \rightarrow G$ with increasing A, i.e., a change from poor to good, to *re-entrant* poor solvent, whereas, at lower ϵ, the sequence of transitions is $E \rightarrow S \rightarrow G$. The conformation changes are directly related to the nature of binding of CI onto the PE. The transition between $S \rightarrow G$ is continuous and associated with critical fluctuations in the shape driven by fluctuations in the fraction of condensed CI. © *2009 American Institute of Physics*. [DOI: 10.1063/1.3078265]

I. INTRODUCTION

The equilibrium properties of a polyelectrolyte (PE) are governed by an interplay between long-range attractive forces between monomers, electrostatic interactions arising predominantly from mobile counterions (CIs), and polymer elasticity. Of these forces, electrostatics has been the most difficult to handle, both analytically and computationally, especially in the regime where the strength of the electrostatic interaction, parametrized by the ratio of the electrostatic condensation energy of the multivalent CIs and thermal energy, is high. While the behavior at high temperature or low electrostatic energy is well described by the mean field Poisson–Boltzmann (PB) theory,[1–3] several computer simulation studies on PE, starting from Ref. 4, reported qualitative deviations from PB at low temperatures or high electrostatic energy.[4–12]

These studies reveal that the main cause for the deviation is that PB theory underestimates the extent of CI condensation at high electrostatic coupling and low temperatures and neglects spatial correlations. For instance, a study of the equilibrium conformations of a PE as a function of charge density and solvent quality (restricting to weak electrostatics and poor solvent conditions), using a Debye–Huckel framework,[7] demonstrated that with increasing charge density the PE globule splits into a string of pearls, in agreement with scaling arguments.[13] Simulations with explicit CI (Ref. 10) verified the above and further showed a collapse of the PE at higher electrostatic coupling, due to attractive, dipolar interactions arising from the condensation of CI onto the monomers. Apart from these studies on free PE, the confor-

mations of a constrained PE, such as a grafted PE, in the regime of low electrostatic coupling were examined using molecular dynamics simulations.[14]

In this paper, we study the equilibrium phase diagram of a grafted PE across a range of electrostatic couplings and solvent quality using Monte Carlo (MC) simulations and scaling arguments. Our study highlights the competition between the monomer-monomer, monomer-CI interactions, and polymer elasticity. As a consequence, the PE exhibits a variety of phases, which we characterize as extended (E), pearls with m beads (P_m), sausage (S), and globular (G). With increasing electrostatic interaction, the PE exhibits the following sequence of conformations: $G \rightarrow P_2 \rightarrow P_3 \rightarrow \ldots \rightarrow S \rightarrow G$. Thus, as a function of increasing electrostatic interaction, we go from poor to good to re-entrant poor solvent. These conformation changes are intimately tied to the nature of binding of CI onto the PE. For weak electrostatic interactions, the CIs condense onto the PE and partially screen the monomer charge. However when the electrostatic interactions are stronger, we find that new composite degrees of freedom, such as dipoles comprising of monomer and CI charges, emerge. In addition, we find that the transition between S to the re-entrant G is continuous and associated with critical fluctuations in the shape driven by fluctuations in the fraction of condensed CI.

II. MODEL AND SIMULATION DETAILS

Our model PE is a linear chain of N spherical beads, of charge e and diameter a, connected through harmonic springs. One end of the PE is anchored to the wall at $x = 0$. To ensure charge neutrality, we introduce N oppositely charged CIs with the same valency and diameter. We neglect hydrodynamic effects and treat the solvent as a dielectric continuum with permittivity κ. The system is bound within a

---
a)Electronic mail: jayasree@physics.iitm.ac.in.
b)Electronic mail: pranjith@curie.fr.
c)Electronic mail: madan@ncbs.res.in.
d)Electronic mail: sunil@physics.iitm.ac.in.

cubic box of volume L^3, with impenetrable, nonpolarizable walls at $x=0$ and $x=L>aN$. We apply periodic minimum image boundary conditions along the y and z directions.[11] We ignore any contribution from image charges at the boundaries along the x-axis.

In our simulation, we model the nonelectrostatic interactions by (i) a Lennard-Jones (LJ) potential,

$$U(r) = \begin{cases} \epsilon_1 \sum_{i<j} \dfrac{a^{12}}{(\mathbf{r}_i - \mathbf{r}_j)^{12}} - 2\dfrac{a^6}{(\mathbf{r}_i - \mathbf{r}_j)^6} & |\mathbf{r_i} - \mathbf{r_j}| < \mathbf{a}, \\[2ex] \epsilon_2 \sum_{i<j} \dfrac{a^{12}}{(\mathbf{r}_i - \mathbf{r}_j)^{12}} - 2\dfrac{a^6}{(\mathbf{r}_i - \mathbf{r}_j)^6} & |\mathbf{r_i} - \mathbf{r_j}| \geq \mathbf{a}, \end{cases}$$

(1)

between all particles and (ii) a harmonic spring potential acting between connected beads of the PE,

$$U_s = \sum_i k(|\mathbf{r}_i - \mathbf{r}_{i+1}| - a)^2,$$

(2)

where we take the spring constant, $k = 800 k_B T/a^2$, for the simulation. For monomer-monomer interaction we choose $\epsilon = \epsilon_1 = \epsilon_2$ and for the CI-CI and monomer-CI interactions $\epsilon_1 = 1$ and $\epsilon_2 = 0$. The electrostatic potential between any pair of beads is

$$U_c = A \sum_{i<j} \frac{a s_i s_j}{|\mathbf{r}_i - \mathbf{r}_j|},$$

(3)

where s_i gives the sign of the ion charge. The electrostatic coupling strength $A = q^2 l_B/a$ measures the ratio of the coulomb to thermal energy when the distance of separation between two charges is a; here q is the valency of the monomer and $l_B = e^2/4\pi\kappa k_B T$ is the Bjerrum length. From now on, we will write all distances in units of a and energy in units of $k_B T$.

We determine the equilibrium conformations and phase diagram of this grafted flexible PE with explicit CIs over a wide range of values of the electrostatic coupling A and LJ parameter ϵ, using the standard MC metropolis scheme. We use the well known umbrella sampling technique[15,16] to obtain the free energy profile of the PE-CI system as function of its radius of gyration, R_g. This method uses a weight function to bias the MC sampling of configuration space in such a way that the less probable states of the system are sampled frequently. In our simulation, we introduce the weight function by adding a harmonic potential $U_w = (1/2)C(R_g - R_0)^2$ to the total energy of the system. By varying R_0, we sample the whole configuration space and measure the distribution of R_g, from which we calculate the free energy $F(R_g)$ of the PE.

III. EQUILIBRIUM PHASE DIAGRAM

The equilibrium phase diagram of the grafted PE, determined by an interplay between interactions (electrostatics and attractive LJ) and entropy (polymer and CI), is fairly subtle and is shown in Fig. 1. We characterize the phases as globular (G), sausage (S), pearls with m-beads (P_m), and extended (E) by the N-dependent scaling of conformational measures, such as the radius of gyration $\langle R_g \rangle$ and the anisotropy of the gyration tensor; typical conformations are shown
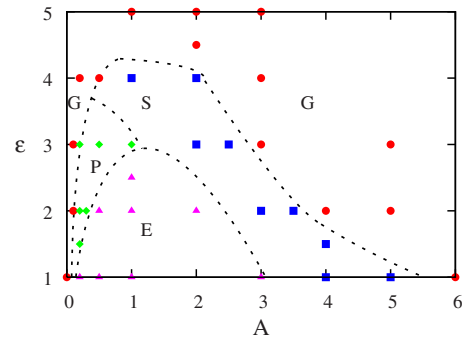

FIG. 1. (Color online) Phase diagram of the PE in the A-ϵ plane for $N = 120$. Different phases are: (i) G: Globular, (ii) P: Pearls, (iii) S: Sausages, and (iv) E: Extended.

in Fig. 3. Let us remind ourselves of the polymer conformations when $A=0$. As a function of ϵ, the polymer goes from being a self-avoiding random coil in good solvent conditions, characterized by the Flory behavior, $\langle R_g \rangle \sim N^{3/5}$, to a collapsed globule (G) in a poor solvent, characterized by $\langle R_g \rangle \sim N^{1/3}$, via a first-order transition at $\epsilon = 1$.[17]

As we turn on the electrostatic interaction, the PE undergoes a sequence of shape changes, depending on the value of ϵ. In the range, $\epsilon < 1$, the PE changes from a self-avoiding random walk to an extended conformation (E), as A varies between 0 and 1.[10,11] This is because, while the electrostatic interaction increases, the CI entropy prevents condensation onto the PE. The net electrostatic interaction between the monomers is repulsive resulting in an extension of the PE and an $\langle R_g \rangle \sim N$. When $A>1$, a finite fraction of CIs condense on the monomers; at $A=5$, for instance, 80% of CI condense onto the PE (Fig. 2). This results in reducing the net monopole charge on each monomer and pairing the monomeric charge with the CI to form dipoles.[10] Such dipoles are the *emergent* degrees of freedom when $A \gg 1$. This leads to an effective attractive interaction and the configuration resembles a sausage (S). As A is increased to 10, complete condensation of the CI takes place, resulting in a collapse into a globule (G). The number of condensed CI at a particular value of A is expected to have a weak dependence on the system size L, as has been shown by previous simulations.[11]
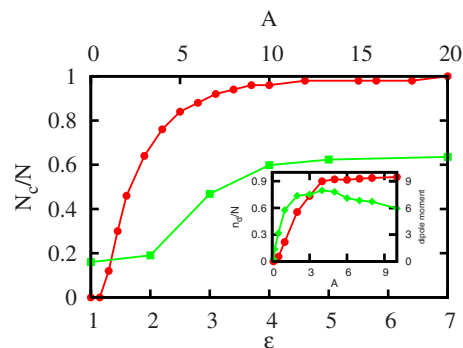

FIG. 2. (Color online) Fraction of condensed CI as a function of (i) the LJ attraction ϵ (square) for $A=1$ and (ii) the electrostatic interaction A (circles) with $\epsilon_1 = 1$ and $\epsilon_2 = 0$. A CI is defined as condensed if it is within a distance $2a$ from any monomer of the PE. The inset shows the net dipole moment of the PE (square) and number of dipoles n_d (circles) as a function of A for $\epsilon = 2$.
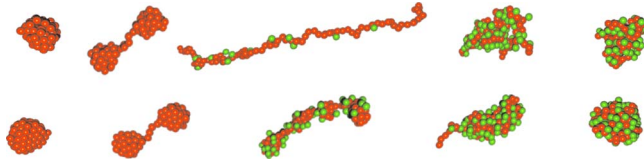
FIG. 3. (Color online) Snapshots of the equilibrium configurations of the grafted PE (red) with condensed CI (green), typical of the different phases. Top panel: For $N=100$, $\epsilon=2$, the configurations from the left are (i) G: Globular at $A=0.1$, (ii) P_2: Pearls with two beads at $A=0.2$, (iii) E: Extended at $A=1$, (iv) S: Sausage at $A=3.5$, and (v) G: Globular at $A=4$. Bottom panel: For $N=120$, $\epsilon=3$, the configurations from the left are (i) G: Globular at $A=0.1$, (ii) P_2: Pearls with two beads at $A=0.2$, (iii) P_4: Pearls with four beads at $A=1$, (iv)S: Sausage at $A=2.5$, and (v) G: Globular at $A=3$.

For larger values of the attractive LJ potential, a new set of phases intervene between the globular phase (G) at $A=0$ and the extended phase (E). These phases occur when $\epsilon \gtrsim 1$ (stronger short range attraction) and $A<1$ (negligible CI condensation), and therefore arise from a competition between short range attractive interactions, long range electrostatic repulsion between monomers, and polymer entropy, akin to the well-known Rayleigh instability. The resulting conformation is a string of pearls with m-beads (P_m), with m increasing with A (Refs. 7, 13, 18, and 19) (see Fig. 3). At large scales, the conformations in the P_m phase is dominated by the electrostatic repulsion between the pearls and the radius of gyration scales as $R_g(N) \sim N$, with a prefactor proportional to the bead size. The subsequent behavior as a function of A depends on the value of the attractive ϵ. In the range $1 < \epsilon < 3$, the PE changes from P_m (where $m \ll N$ is the maximal allowed by the finite size of the polymer) to an extended (E) conformation, as A increases toward 1. This is because the attractive interactions are not strong enough to compete with the increasing electrostatic (monomer-monomer) repulsion as A increases. In this range of ϵ, the conformation then changes from $E \rightarrow S \rightarrow G$, as described in Fig. 3. As we increase the attraction $\epsilon \gtrsim 3$, we lose the extended phase entirely, and the PE goes from $G \rightarrow P_2 \rightarrow P_3 \rightarrow \ldots S$, and subsequently to a re-entrant G phase as we tune the electrostatic repulsion A as shown in Fig. 3.

The conformations at large A, namely, the S and the reentrant G phases, are a consequence of the emergent dipole degrees of freedom. In the inset of Fig. 2 we plot the net dipole moment and the fractional number of emergent dipoles (n_d/N) of the PE as a function of A for $\epsilon=2$. The dipole moment shows a maximum before the globular phase is reached–at this stage, the number of dipoles is small. As we increase A, the number of dipoles increase, but the net dipole moment starts to decrease, as the PE conformation gets more compact in the G phase. The scaling of the radius of gyration in the two G-phases (at low and high A) is the same—$R_g(N) \sim N^{1/3}$ (poor solvent!), as shown in Fig. 4. Thus, the re-entrant G-phase, while structurally similar to the initial G-phase at $A=0$, is different only in its electric dipole characteristics.

At larger values of the attractive potential $\epsilon \gtrsim 4$, the PE conformations go directly from $G \rightarrow S \rightarrow G$ or even from $G \rightarrow G$ at still higher values of $\epsilon \gtrsim 5$, where the latter G-phase has a dipole moment. These direct transitions are consistent with the behavior of the fraction of condensed CI, which
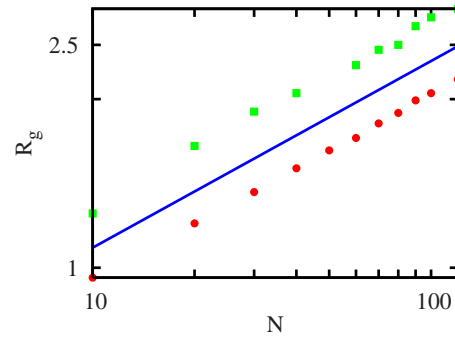

FIG. 4. (Color online) Scaling of the mean radius of gyration $\langle R_g \rangle$ with N for the globular configurations shown in Fig. 3. The circles are for $\epsilon=3.0$, $A=0.1$ and squares are for $\epsilon=3.0$, $A=3.0$. The solid line is a guide to the eyes with $\langle R_g \rangle \sim N^{1/3}$.

increases with ϵ for a fixed A (Fig. 2). The enhancement of CI condensation, which is a result of electrostatic correlations, results in a strong screening of the monomer-monomer interactions.

Before we end this section, a word about finite size effects: In our simulations on finite PEs, the scale for the maximum bead number in the P_m phase is set by system size, and in the thermodynamic limit of $N \rightarrow \infty$, there should be a finite fraction of beads. At this stage we are unsure about how the phase boundaries discussed above would shift as we increase N, or even whether the S phase exists in the thermodynamic limit.

IV. CONTINUOUS TRANSITION FROM $S \rightarrow G$: ANOMALOUS FLUCTUATIONS OF THE SAUSAGE

The phase diagram (Fig. 1) shows a transition from (reentrant) $G \rightarrow S$, upon *reducing* the electrostatic coupling A from a high value. This transition is a symmetry breaking transition; the appropriate order parameter characterizing the spontaneous breaking of spherical symmetry is the *asphericity* parameter, $\langle Y \rangle \equiv 2\langle \lambda_1^2 \rangle / (\langle \lambda_2^2 \rangle + \langle \lambda_3^2 \rangle) - 1$, where $\{\lambda_1, \lambda_2, \lambda_3\}$ are the eigenvalues of the gyration tensor of the PE, with λ_1 as the largest. The asphericity $\langle Y \rangle = 0$ for a globule. Figure 5
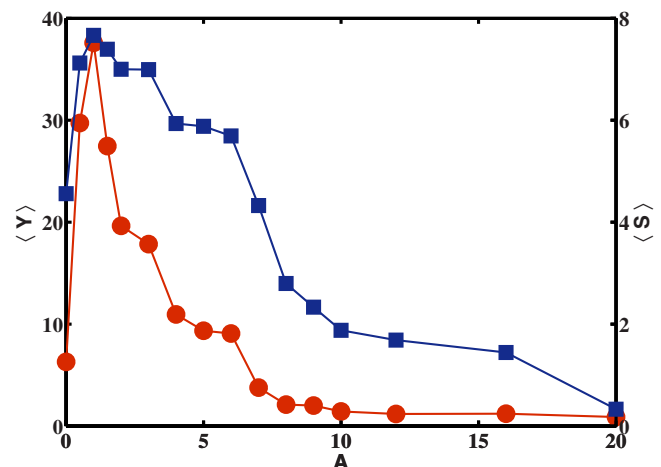

FIG. 5. (Color online) Asphericity $\langle Y \rangle$ (circles) and $\langle S \rangle = \langle R^2 \rangle / \langle R_g^2 \rangle - 2$ (squares) (see text), as a function of electrostatic coupling A, $\epsilon_1=1.0$, $\epsilon_2=0.0$, for $N=50$. For reference, $Y=0$ for a globule, $\langle S \rangle = 4$ for a Gaussian chain, and $\langle S \rangle = 10$ for a rigid rod.
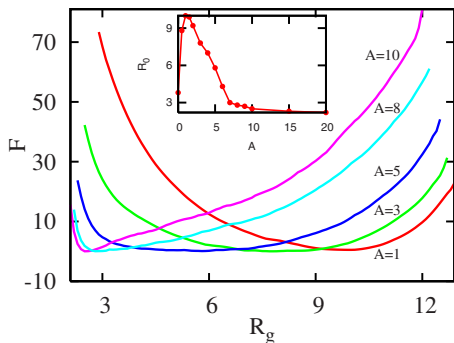
FIG. 6. (Color online) Free energy $F(R_g)$ for different coupling constants of a $N=50$ and $L=50$ PE, for $\epsilon_1=1.0$ and $\epsilon_2=0.0$. (inset) R_0, the value of R_g at which the free energy is the minimum as a function of A, showing smooth change.
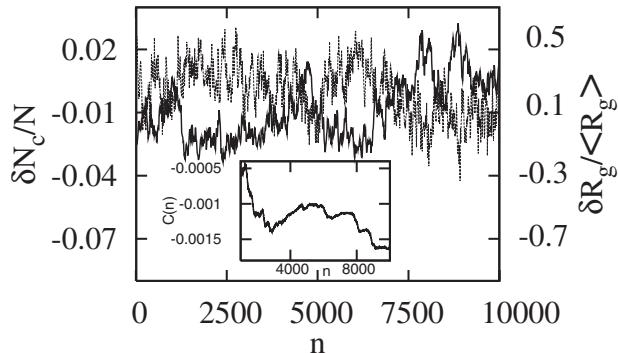

FIG. 8. The deviation of fraction of condensed CI from its average value $\delta N_c/N$ (dotted line) and the deviation of $R_g/\langle R_g \rangle$ from its average value $\delta R_g/\langle R_g \rangle$ (solid line) for different equilibrium configurations with $A=5$, $\epsilon=1$ is shown. The cross correlation $C(n)$ is shown in the inset.

shows how this asphericity changes as a function of A. At the $G \to S$ transition, this symmetry breaking order parameter changes continuously, suggesting a second-order phase transition. On the other hand the $G \to E$ transition at small A seems abrupt, suggesting a first-order transition. We also plot the structural quantity $\langle S \rangle \equiv \langle R^2 \rangle / \langle R_g^2 \rangle - 2$, where R is the squared end-to-end distance,[20,21] as a function of A; this quantity is $\langle S \rangle = 4$ for a Gaussian chain and $\langle S \rangle = 10$ for a rigid rod.

To understand the nature of the phase transitions better, we compute the free energy of the PE with the CI, as a function of R_g for different values of A. The smooth variation in the free energy profile and its minimum with increasing A (Fig. 6), as one moves from $E \to S \to G$, is consistent with the continuous transition described above. Indeed at around $A \sim 5$, when we are in the S-phase, the minima in the free energy profile are extremely shallow, suggesting that the fluctuations of shape in this regime would be large, consistent with its proximity to a critical point. We note that the variation in R_0 with A (shown in inset of Fig. 6) is very similar to that of free polymer,[10,11] indicating that the grafting has little or no effect on the collapse transition.

We explicitly study the fluctuations in the configurations of the S-phase; snapshots of the equilibrium configurations, displayed in Fig. 7, show very strong shape fluctuations, with significant sampling of both extended and collapsed conformations. These large fluctuations of the PE shape in the S-phase are accompanied by strong fluctuations in the fraction of condensed CI (Fig. 8). The dynamical interplay between the PE shape and condensed CI is shown in Fig. 8; whenever there is a transient enhancement of the condensed CI fraction, the PE chain gets more compact (owing to the effective dipolar attraction) and, whenever the condensed fraction is low, the chain gets stretched out

(owing to strong monomer-monomer repulsion) leading to a large negative value of the cross correlator, $C(n) = (1/n)\Sigma_{i=1}^{n}(\delta N_c(i) \delta R_g(i))/(\langle R_g \rangle N)$, where n is the number of MC steps.

To quantify these fluctuations as a function of A we compute the second moment of R_g, $\langle \delta R_g^2 \rangle = \langle (R_g - \langle R_g \rangle)^2 \rangle$, using the free energy $F(R_g)$. This quantity shown in Fig. 9 exhibits a peak around $A=5$ (in the S regime), with its height increasing with system size, indicating a critical point. The cross correlator, $\langle \delta R_g \delta N_c \rangle$, shows a negative peak at exactly where the peak in $\langle \delta R_g^2 \rangle$ appears, reiterating the interplay between PE shape and condensation of CI. Our preliminary study to determine the order of the phase transition needs to be reinforced by a more detailed study of the scaling of fluctuations as a function of chain length N; we hope to return to this when we have better computational facilities at our disposal. However, if we take our study as evidence of a continuous transition, then this would imply that upon increasing ϵ, the critical line would necessarily terminate in a critical end point.

V. CONCLUSION

Using extensive MC simulations, we explored the phase diagram of a grafted PE with explicit CIs as a function of the electrostatic coupling A and LJ interaction parameter ϵ. We characterized the phases in terms of the statistics of their conformations and electrostatic measures, such as fraction of condensed CIs. We uncovered four distinct phases: Globular, string of pearls with m-beads, extended, sausage, and re-

FIG. 7. (Color online) Configuration snapshots of the sausage (S) showing strong fluctuations at equilibrium for $A=5$, $\epsilon=1$. The configurations change from being extended to collapsed.
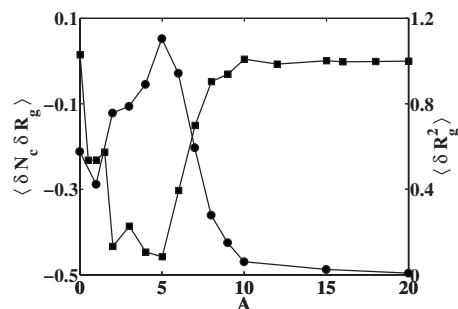

FIG. 9. The deviation of R_g from its average value $\langle \delta R_g^2 \rangle$ (circle) and the cross correlator $\langle \delta R_g \delta N_c \rangle$ (square) as a function of A for $\epsilon_1=1.0$, $\epsilon_2=0.0$.

entrant globule with nonzero dipole moment. As we noted, the effect of grafting the PE at one end is negligible when the electrostatic interaction A is large. Thus the large A region of the phase diagram shown in Fig. 1 should be valid for the free PE too (in contrast, Ref. 7 explores the low A regime of free PE).

Our study, which treats the CI explicitly, highlights the strong correlation between collapse of the PE and the condensation of the CI. The dependence of CI condensation on ϵ (at low values of A), the emergent formation of dipoles from condensation of CI onto the PE, the anomalous fluctuations of the sausage, are all a consequence of these correlated ion effects. The appearance of new degrees of freedom, viz., dipoles, when $A > 1$, makes it difficult to construct an analytical theory valid for all values of A. One possible approach would be to represent the CI by "two-species," a monopole charge density and a dipole density, whose relative fraction depends on A. We will explore these ideas in a future submission.

ACKNOWLEDGMENTS

[1] N. V. Brilliantov, D. V. Kuznetsov, and R. Klein, Phys. Rev. Lett. **81**, 1433 (1998).
[2] N.-K. Lee and S. Obukhov, Europhys. Lett. **66**, 350 (2004).
[3] M. Muthukumar, J. Chem. Phys. **120**, 9343 (2004).
[4] M. Deserno, C. Holm, and S. May, Macromolecules **33**, 199 (2000).
[5] M. Stevens and K. Kremer, Phys. Rev. Lett. **71**, 681 (1993).
[6] R. Winkler, M. Gold, and P. Reineker, Phys. Rev. Lett. **80**, 3731 (1998).
[7] A. V. Lyulin, B. Dunweg, O. V. Borisov, and A. A. Darinskii, Macromolecules **32**, 3264 (1999).
[8] H. J. Limbach and C. Holm, J. Chem. Phys. **114**, 9674 (2001).
[9] H. J. Limbach and C. Holm, Comput. Phys. Commun. **147**, 321 (2002).
[10] S. Liu and M. Muthukumar, J. Chem. Phys. **116**, 9975 (2002).
[11] R. R. Netz, Phys. Rev. Lett. **90**, 128104 (2003).
[12] H. Wada, Y. Murayama, and M. Sano, Phys. Rev. E **72**, 041803 (2005).
[13] A. V. Dobrynin, M. Rubinstein, and S. P. Obukhov, Macromolecules **29**, 2974 (1996).
[14] P. A. Crozier and M. J. Stevens, J. Chem. Phys. **118**, 3855 (2003).
[15] G. M. Torrie and J. P. Valleau, Chem. Phys. Lett. **28**, 578 (1974).
[16] J. S. van Duijneveldt and D. Frenkel, J. Chem. Phys. **96**, 4655 (1992).
[17] P. G. de Gennes, J. Phys. (France) Lett. **39**, 299 (1978).
[18] Y. Kantor and M. Kardar, Phys. Rev. E **51**, 1299 (1995).
[19] H. Schiessel and P. Pincus, Macromolecules **31**, 7953 (1998).
[20] F. Csajka and C. Seidel, Macromolecules **33**, 2728 (2000).
[21] R. R. Netz, J. Phys. Chem. B **107**, 8208 (2003).